





Indirect-to-direct band-gap transition in few-layer β -InSe as probed by photoluminescence spectroscopy

B. R. Borodin, I. A. Eliseyev , A. I. Galimov , L. V. Kotova, M. V. Durnev, T. V. Shubina , M. A. Yagovkina, and M. V. Rakhlin *

Ioffe Institute, St. Petersburg 194021, Russia



(Received 29 September 2023; accepted 13 December 2023; published 4 January 2024)

InSe is a promising material for next-generation two-dimensional electronic and optical devices, the characteristics of which are largely determined by the type of band structure, direct or indirect. In general, atomic force microscopy and optical methods can be sensitive to peculiarities of the electronic structure, leading to different results. In this work we will focus on the luminescent properties of few-layer β -InSe with a thickness of 6–75 monolayers (MLs). Low-temperature micro-photoluminescence (μ -PL) studies show a sharp increase in PL intensity in the range of thicknesses from 16 to 20 monolayers, where, in addition, there is a singularity in the dependence of the work function on the thickness. Time-resolved photoluminescence spectroscopy reveals three characteristic PL decay times that differ from each other by about an order of magnitude. We associate the processes underlying the two faster decays with the recombination of electrons and holes between the band extrema, either directly or through the interband relaxation of holes. Their contributions to the total PL intensity increase significantly in the same thickness range, 16–20 MLs. On the contrary, the slowest contribution, which we attribute mainly to the defect-assisted recombination, prevails at a smaller number of monolayers and then noticeably decreases. These results indicate the indirect-to-direct band-gap transition near 16–20 MLs, which determines the range of applicability of few-layer β -InSe for efficient light emitters.

DOI: [10.1103/PhysRevMaterials.8.014001](https://doi.org/10.1103/PhysRevMaterials.8.014001)

I. INTRODUCTION

The booming development of the field of two-dimensional (2D) materials has led to the emergence of several classes of layered materials designed for various applications [1–5]. Among them, the post-transition-metal chalcogenides (PTMCs), such as InSe and GaSe, are very promising from both a fundamental and applied perspective [6–9]. In contrast to transition-metal dichalcogenides [10,11], PTMC monolayers have an indirect band gap that transforms to direct with increasing thickness. This transition is related to the change of the valence-band dispersion: parabolic dispersion specific to bulk PTMCs turns into “Mexican hat” dispersion in monolayers [12–16].

The “Mexican hat” dispersion of holes with an extremum loop results in many unique electronic properties and physical phenomena in PTMCs [17–22]. Among PTMC materials, InSe is the most actively studied, as it has many possible applications in high-mobility electronic devices [6,7,23,24], spintronics [22,25,26], optoelectronics [8,27,28], flexible devices [9,29,30], and straintronics [31–34]. However, despite significant progress in the fundamental and application-related studies of InSe, the optical properties of a few-layer InSe are still poorly understood. Of particular interest is the transition between indirect and direct band gaps and its influence on the photoluminescence (PL) of InSe layers. Theoretical works predict a smooth transformation of the band

gap from indirect to direct as the number of layers increases from 1 to about 20 [14,16,22,35]. Meanwhile, experimental data are controversial. Studies of the optical properties show different PL dynamics with increasing thickness and the presence of PL already starting from two monolayers (MLs) [36–41]. The study of γ -InSe band structure evolution using angle-resolved photoemission spectroscopy by Hamer *et al.* indicates that after the thickness of 3 ML, the band inversion is no longer measurable as it is less than kT at room temperature [42]. There are several reasons for these discrepancies. The first reason is the presence of four different InSe polytypes (γ -, ϵ -, β - and δ -phases), which have different crystallographic structures and, hence, slightly different electronic and optical properties. The vast majority of experimental works are dedicated to γ -InSe [37–39], while a part of works does not specify the polytype [40,41]. On the other hand, few-layer β -InSe is much less studied, despite the unique excitonic properties of the bulk material [43,44]. The second reason is the noncryogenic temperatures of most experiments. According to theoretical calculations [13,14,16,22,35,45], the valence band changes smoothly in the transition region, and hence, the high kT energy can blur the moment of transition. The third reason is the natural oxidation of InSe under ambient conditions, which creates different types of defects involved in optical and electronic processes [24,41,43,46–48].

In general, different methods can be sensitive to different aspects of the electronic structure and therefore can detect the transition from indirect to direct band gap at different numbers of monolayers for a given polytype, which is an important factor for designing optoelectronic devices. In this work we

*maximrakhlin@mail.ru

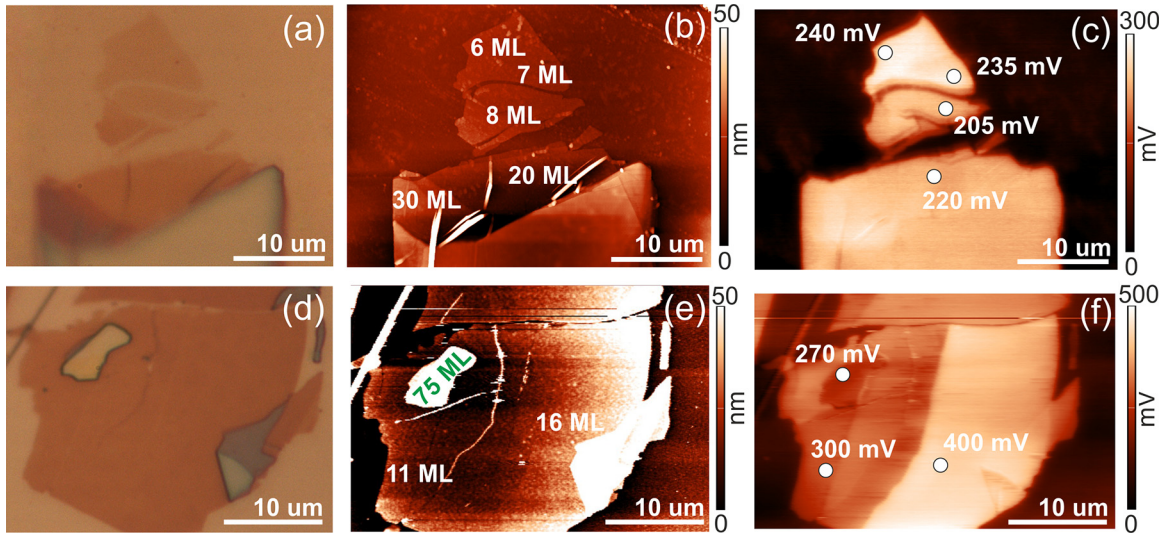


FIG. 1. Optical images (a), (d), topography (b), (e), and surface potential distribution (c), (f) of the selected flakes. Flake thicknesses estimated from the AFM data are indicated on the topography maps.

use PL spectroscopy at cryogenic temperature to detect the transition from indirect to direct band gap in a few-layer β -InSe. The samples were first studied by Raman spectroscopy, atomic force microscopy (AFM), x-ray diffraction (XRD), and Kelvin probe force microscopy (KPFM), and all methods showed a singularity in the dependence of work function at a flake thickness of 16–20 ML. The combination of XRD and Raman spectra allowed us to reveal the β -polytype of the studied samples. The KPFM measurements of InSe on a metal substrate are performed in this work, which allowed us to obtain the absolute values of the work function. Microphotoluminescence (μ -PL) demonstrated a sharp increase in the PL intensity in flakes of the same (16–20 ML) thickness range, which we explained by the dominance of direct optical transitions. Note that the previously reported data on γ -InSe showed that the γ -phase flakes become direct-gap at much lower $N \approx 8$ ML [39]. Additional information was obtained using time-resolved photoluminescence (TRPL), which, surprisingly, shows three characteristic PL decay times that differ from each other by about an order of magnitude. In contrast to previous TRPL measurements, we were able to accurately determine the slow components of the decay curves. We attribute the processes underlying the two faster PL decays to direct-band recombination of electrons and holes (either free or bound in exciton), which occurs either immediately between band extrema or with the participation of interband hole relaxation. The slowest decay is due to a combination of defect-assisted and possibly indirect optical transitions; the latter component disappears when the direct type of band structure is finally established. The simultaneous increase in the contributions of two faster direct transitions emphasizes the transformation of the valence band from the “Mexican hat” to the parabolic one, probed by PL.

II. SAMPLES

The structures under study were fabricated from a commercially available, high-quality InSe bulk crystal. Silicon wafers coated with 50-nm-thick gold were used as substrates.

For sample preparation, the so-called Scotch tape method was used.

After fabrication, the topography of the samples was studied using AFM. Several flakes were selected based on their thickness. We picked flakes with thicknesses ranging from 6 to 75 to investigate the evolution of electronic and optical properties of a few-layer β -InSe. The optical images of the flakes are shown in Figs. 1(a) and 1(d), while Figs. 1(b) and 1(e) demonstrate the topography of the selected flakes with the indicated number of layers as it was measured by AFM.

As seen from Fig. 1, the obtained flakes are sufficiently large, which makes it possible to obtain reliable data on PL and surface potential. Figures 1(c) and 1(f) show the surface potential distribution maps. We can see that the surface potential depends nonmonotonously on the thickness and even experiences leaps between pairs of flakes of a certain thickness. While random jumps of 5 and 30 mV between, respectively, flakes of 6–7 ML and 7–8 ML may reflect the influence of the surface or substrate, a jump of 180 mV between flakes of 16 and 20 ML indicates a cause possibly related to the transformation of band structure. We believe that if such a rapid change in the surface potential indicates this transformation, then it should also manifest itself in the optical properties. To confirm this assumption, we studied flake PL, since both intensity and characteristic decay times should depend on the type of band gap, whether direct or indirect.

Figure 2(a) shows a typical x-ray diffraction (XRD) pattern of the bulk InSe crystal used for exfoliation. The periodic peaks indicate a perfect stacking of the layers along the z axis for InSe crystal. The cell parameter was indexed to be $c = 1.66$ nm, indicating that the stacking period is composed of two atomic layers. Thus the studied InSe samples feature 2H phase and therefore should either be β or ϵ polytype (see also Ref. [49] for XRD determination of the InSe polytype). For further investigation we performed the measurements of the second-harmonic generation in the bulk sample. The crystal stacking of the β -InSe is described by the point group D_{6h} ,

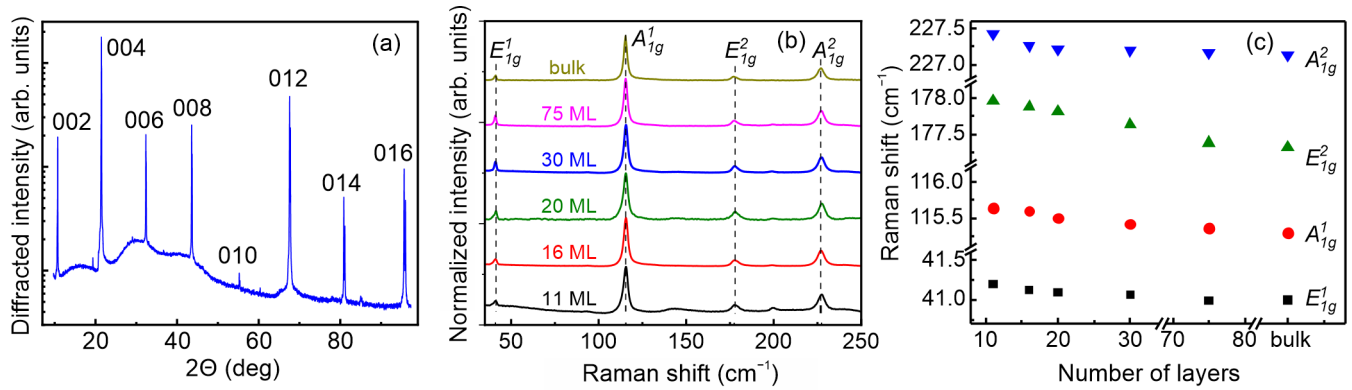


FIG. 2. (a) The XRD pattern of the bulk InSe crystal. (b) Unpolarized Raman spectra as a function of number of InSe MLs. The spectra are normalized to the intensity of the A_{1g}^1 line, and the dashed lines show peak positions for bulk InSe. (c) Raman shifts for InSe as a function of number of MLs.

which has an inversion center and hence the second-harmonic generation from the β -InSe is forbidden under the electric dipole approximation [50]. On the other hand, ϵ -InSe is described by the D_{3h} point group without an inversion center and is expected to generate the second-harmonic signal. Since our sample did not demonstrate any second-harmonic signal, we conclude that the bulk sample and the studied flakes made of it are β polytype.

The structural properties of the samples were investigated by means of micro-Raman spectroscopy. Figure 2(b) represents the spectra measured in the areas with thicknesses of 11–75 MLs (based on AFM data) and a spectrum of the bulk sample used for exfoliation. All the spectra demonstrate features characteristic of β -InSe [13,51]: E_{1g}^1 ($\sim 41 \text{ cm}^{-1}$), A_{1g}^1 ($\sim 115 \text{ cm}^{-1}$), E_{1g}^2 ($\sim 178 \text{ cm}^{-1}$), and A_{1g}^2 ($\sim 227 \text{ cm}^{-1}$) lines. With decreasing thickness, we observe a monotonous increase of the frequencies of all the lines [Fig. 2(c)], which is consistent with the general trend demonstrated in previously published works on InSe with varying thickness [52,53]. We also observe for some flakes a small contribution of the normally Raman-silent line corresponding to the A_{2u} phonon ($\sim 200 \text{ cm}^{-1}$), which may be due to the presence of strain in the crystal lattice [44]. The line observed for 11-ML flakes at $\sim 145 \text{ cm}^{-1}$ can correspond to the A_{2u} phonon of monoclinic InSe [44]. However, the fraction of monoclinic phase turns out to be small, since we did not observe any additional PL peaks at 1.88 eV, which is characteristic of monoclinic InSe.

III. EMISSION PROPERTIES

A. Micro-photoluminescence

Figure 3(a) demonstrates the PL spectra of the flakes obtained at 4 K. One can see that both the spectral behavior and the PL intensity (characterized by a noise track) strongly depend on the InSe thickness. The integrated PL intensity and the work function vs the number of layers are summarized in Fig. 3(b). There is no detectable PL signal for 6- and 7-ML flakes. PL appears in an 8-ML flake and slowly increases up to 16-ML thickness. In a 20-ML flake, PL intensity increases abruptly and then grows linearly from 20 to 75 MLs. We also observed a similar behavior of the PL intensity on InSe

flakes on SiO_2 [see inset in Fig. 3(b)]. However, a sharp increase in the PL intensity of InSe on the gold substrate is observed after 16 layers, while for the SiO_2 substrate this effect is observed after 24 layers. It can be connected with oxidation of the sample on the SiO_2 substrate, as this sample was exposed to ambient conditions for a significant amount of time so that the actual thickness of these flakes might be smaller than the AFM indicated. We believe that the absence of PL for thin flakes (< 8 ML) is associated with the dominant role of surface defects, which are common for InSe exposed to ambient conditions [54]. These defects provide a nonradiative recombination channel. Also, the influence of the metal when using Au/Si substrates cannot be ruled out. With the thickness increase (≥ 8 ML), the role of volume increases and weak PL appears. As described above, the work function behaves nonmonotonously with the number of layers and varies between 4.6 and 4.8 eV. Its sharp decrease occurs at about 20 mV, and then an increase follows with a decrease in the number of layers, probably due to enhanced size quantization [35]. The singularity at 16–20 ML agrees well in terms of the layer number with a sharp increase in the PL intensity. Superlinear growth of the PL intensity with increasing thickness has been previously observed in InSe flakes of different polytypes [37–41] and has been attributed to the transition between indirect and direct band gap in InSe. Density functional theory (DFT) calculations predict the valence-band dispersion in InSe to change from the Mexican-hat-shaped (or ring-shaped) to the parabolic-shaped with increasing number of layers [13,14,45]. For the “Mexican hat” valence-band configuration expected for InSe, for layer thicknesses from one to several MLs, the band gap is indirect. Based on the analysis of the steady-state and time-resolved (discussed below) PL, we conclude that the flakes with $N \leq 16$ have an indirect band gap. Hence we attribute the rapid increase of PL intensity in the 16–20 ML interval, see Fig. 3(b), to the transformation of the valence band and indirect-to-direct band-gap transition. The obtained results are consistent with the theoretical calculations obtained by Rybkovskiy *et al.* [14]. The smooth PL growth in the 8–16 and 20–75 ML intervals is associated with an increase of the emitting volume. Note that the work-function leap between 16 and 20 ML correlates with the rapid increase of PL in the same flakes.

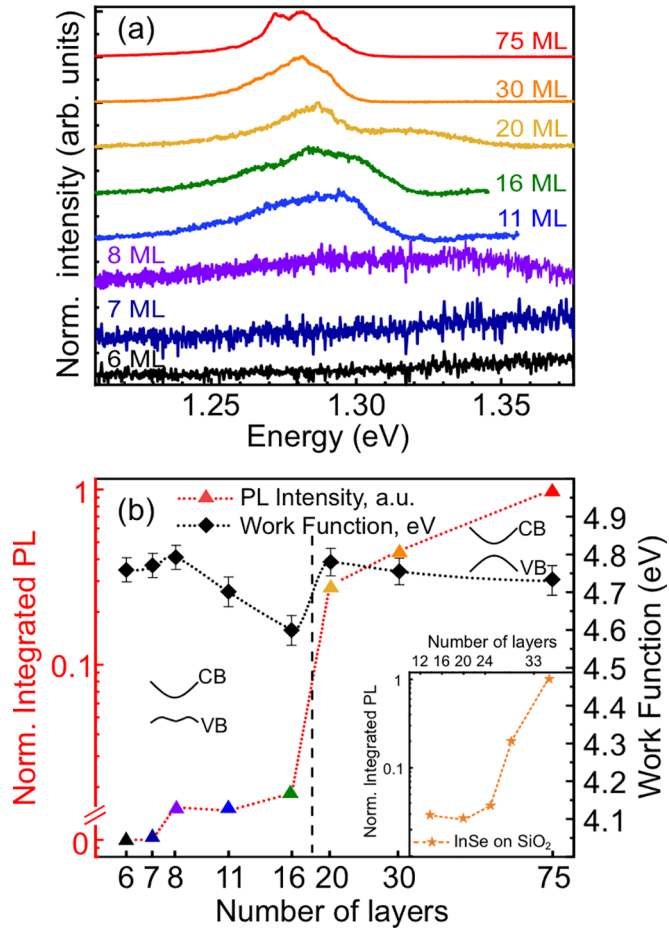


FIG. 3. (a) PL spectra of the flakes with different thicknesses at 4 K. Each spectrum is normalized to its maximum and shifted vertically for clarity. (b) Integrated PL intensity normalized to its value at 75 ML and the work function in flakes with different thickness. The black dashed line shows an approximate area of indirect-to-direct band-gap transition. The insets show normalized integrated PL intensity of InSe on SiO₂.

B. Time-resolved photoluminescence

The broad low-temperature PL spectra shown in Fig. 3(a) indicates a possible contribution of the defect-assisted

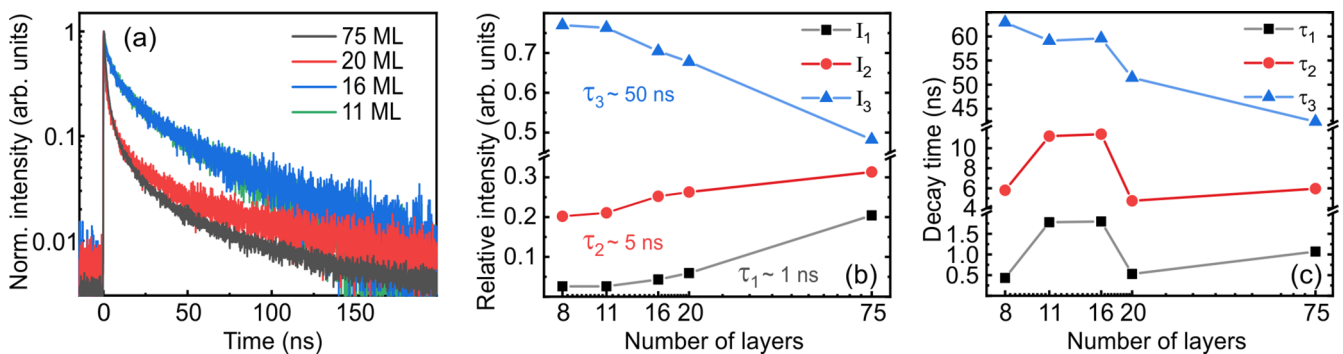


FIG. 4. (a) Normalized PL decay curves measured from four InSe flakes with different thicknesses. (b) Relative intensities of the “fast” (I_1/I), “medium” (I_2/I), and “slow” (I_3/I) components of PL as a function of number of layers. Corresponding decay times are marked on the graph. (c) Decay times τ_1 , τ_2 , and τ_3 as a function of the number of layers.

radiative recombination, which has been mentioned in previous optical studies of few-layer and bulk InSe [39,41,43]. To gain a further insight regarding the nature of PL, we use the TRPL spectroscopy. As far as we know, only Venanzi *et al.* have experimentally determined the decay times in InSe [41], but the measurement range was insufficient to accurately determine the long components of the decay curves, so we used a laser with 4 MHz frequency to refine their data. Figure 4 shows the results of TRPL measurements in four flakes of 8, 11, 16, 20, and 75 MLs. For all the studied thicknesses, the best fit for the decay curve was achieved using three exponential components, which were considered as corresponding to the PL itself, convoluted with the instrumental function (for a procedure description, see [55]). The function used for the fit has the form

$$f(t) = i_1 e^{-t/\tau_1} + i_2 e^{-t/\tau_2} + i_3 e^{-t/\tau_3}, \quad (1)$$

where τ_j are the characteristic decay times, and i_j are the corresponding PL intensities, $j = 1, 2, 3$. The total (time-integrated) intensity of the j th component is given by $I_j = i_j \tau_j$. Figures 4(b) and 4(c) show the relative intensities of each component given by I_j/I , where $I = I_1 + I_2 + I_3$, and the decay times τ_j are functions of the number of layers.

C. Optical transitions

The first component of the PL decay, referred to as “fast,” has a characteristic decay time $\tau_1 \sim 0.5 - 1$ ns, the second, “medium,” component decays at the timescale of $\tau_2 \sim 4-11$ ns, and the third, “slow,” component decays in $\tau_3 \sim 40-60$ ns, see Fig. 4(c). We attribute part of the “slow” component to the defect-related recombination, as mentioned in previous studies of thin-layer InSe [41]. In this case, an electron or/and a hole are localized at defects, which results in a small overlap of their wave functions in the coordinate or momentum space. This, in turn, leads to a small radiative recombination rate and, consequently, large decay time τ_3 . The line associated with the defects is located somewhat below the emission of the free exciton, and during measuring the TRPL, we must inevitably register a part of that. The other part of the “slow” component might be ascribed to the indirect exciton transition situated a bit above. As with any indirect transition, it is slow, especially at low temperature when the phonon population is poor. While the defect-related contribution is weakly

dependent on the flake thickness, the fundamental indirect part should strongly follow the indirect-to-direct transition. Our data for few-layer InSe obtained is in line with that.

As shown in Fig. 4(b), the relative contribution of the defect-assisted processes to the total PL (I_3/I) is large and, in fact, dominates the PL at $N \leq 20$. However, as the critical thickness of 16–20 ML is approached, the contribution of the “slow” component decreases. The remainder is due to defect-related radiation captured due to our measurement conditions. At the same time, a gradual increase in two “faster” components is observed, the presence of which, as will be described below, is due to the specific band structure of InSe.

We assume that the “faster” component of the PL decay (I_1 and τ_1) is due to the direct band-to-band recombination of electrons and holes (either free or bound in exciton). The decay rate τ_1^{-1} includes both radiative and nonradiative processes, the latter being, e.g., the capture of a free electron or hole to a defect. The radiative lifetime τ_r can be estimated from $\tau_r^{-1} = 4\omega^3 d_z^2 / (3\hbar c^3)$, where ω is the transition frequency, d_z is the matrix element of the electric dipole moment between the conduction- and valence-band states at $\mathbf{k} = 0$, \hbar is the Planck constant, and c is the speed of light. Using $\hbar\omega = 1.3$ eV and $d_z/e = 6 \text{ \AA}$ [45], we obtain $\tau_r \approx 3$ ns, in reasonable agreement with experimental values of τ_1 .

As shown in Fig. 4(b), for 8, 11, and 16 ML, the PL is dominated by the “slow” component. However, starting from 20 ML, the relative contribution of the “fast” component (I_1/I) to PL significantly increases, up to 20% in the 75-ML flake. Since the “fast” component is attributed to the band-to-band radiative recombination, such an increase indicates the transition to the direct-band-gap InSe, which takes place in the region of 16–20 ML. Note that, however, the defect-assisted contribution still remains large, even in the flakes with the direct band gap.

IV. DISCUSSION

Let us now discuss the optical transitions and electron/hole relaxation in a few-layer InSe, which sheds light on the appearance of the I_2 with a longer decay time. Bulk β -InSe is described by the point-symmetry group D_{6h} , whereas the symmetry of a few-layer structure depends on the number of layers. Flakes with even-layer thickness belong to the centrosymmetric D_{3d} group, while flakes with odd-layer thickness belong to the noncentrosymmetric D_{3h} group [14,43,45,56,57]. At the Γ point of the Brillouin zone, the electronic states of the topmost valence band (v) transform as scalar functions corresponding to the Γ_1^+ and Γ_1 irreducible representations in the even-layer and odd-layer structures, respectively. The states of the lowest conduction band (c) transform as the z component of the vector, i.e., according to the Γ_2^- and Γ_4 representations [14,43,45,58], see Fig. 5. Therefore the electric dipole transitions between the v and c bands are possible for electric fields polarized in the z direction, $\mathbf{E} \parallel \mathbf{z}$. Note that spin-orbit coupling also allows for weak $c \rightarrow v$ transitions in the x and y polarizations [58]. The valence bands with lower energies, $v1$ and $v2$, are formed by the states that transform as $x \pm iy$ and $z(x \pm iy)$, respectively. The corresponding representations of the D_{3d} (even N) and D_{3h} (odd N) groups are Γ_3^- and Γ_6 for the $v1$ valence band

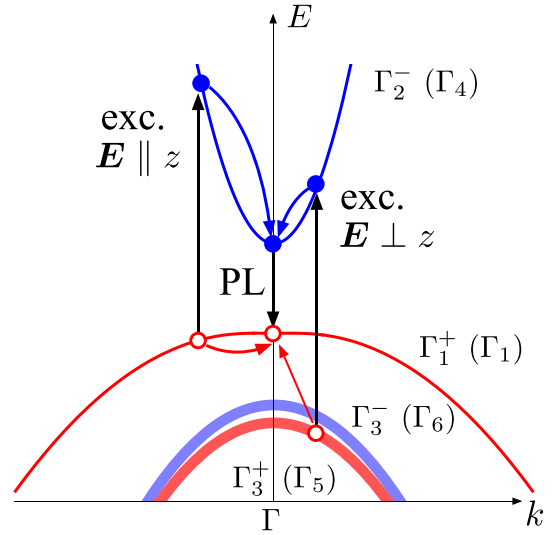


FIG. 5. The scheme of excitation, relaxation, and emission processes in a multilayer direct-band InSe at high excitation energy. The black arrows show optical transitions with absorption or emission of light; the blue and red arrows show the energy relaxation processes in the conduction and valence bands, respectively. Γ_j^\pm and Γ_j denote the irreducible representations of the D_{3d} (even number of monolayers) and D_{3h} (odd number of monolayers) point groups, respectively, which describe the shown bands at the Γ point.

and Γ_3^+ and Γ_5 for the $v2$ valence band, respectively [14,45]. Electro-dipole optical transitions are allowed between $v2$ and c bands for the electric field lying in the plane of the layer, $\mathbf{E} \perp \mathbf{z}$, see Fig. 5.

Figure 5 schematically shows the band structure and excitation and relaxation processes in direct-band-gap InSe flakes. In our TRPL experiment, the excitation photon energy is approximately 3 eV, which is high enough to excite both the $v \rightarrow c$ and $v2 \rightarrow c$ transitions (also referred to as A and B lines, respectively [38,45]). The kinetics of relaxation is different for these two transitions. For the A transition, photoexcited electrons and holes rapidly relax to the band extrema, where they recombine radiatively with the rate τ_1^{-1} . This process governs the “fast” decay component of PL shown in Fig. 4. In the case of the B transition, the photoexcited hole resides in the lower $v2$ band and, in order to recombine with an electron, should at first relax to the topmost valence band. This interband energy relaxation is slow, since it requires phonon-assisted transitions between different valence subbands and hence governs the corresponding PL decay time. This hole relaxation might be responsible for the “medium” decay component in Fig. 4 and the corresponding relaxation time τ_2 , although this assumption requires further investigation.

It should be noted that any multiexponential fitting cannot give precise boundaries between the areas of action of various mechanisms that interpenetrate, overlap, and influence each other. Therefore our consideration is of a qualitative nature, although the main observation of the band structure transformation from indirect to direct in a certain thickness range (16–20 ML) is beyond doubt.

V. CONCLUSIONS

To conclude, we have experimentally investigated the optical properties of a few-layer β -InSe at cryogenic temperature. Using the exfoliation technique, we have prepared flakes with different thicknesses varying in the 6–75-ML range. XRD measurements and Raman spectra of the bulk InSe crystal used for exfoliation have shown that the studied sample has the β -type crystal structure. Kelvin probe force microscopy has revealed rapid jumps of the work function between the 16-ML and 20-ML flakes, indicating a possible transformation of the electronic structure. We have observed a rapid, more than an order of magnitude increase of the PL intensity in the same 16–20 ML interval. We attribute these rapid changes of the work function and PL signal to the transformation of the valence-band configuration from the “Mexican hat” to the parabolic one in a 20-ML flake. To uncover the PL mechanisms in our samples, we have performed the time-resolved PL measurements. We have found that for all the studied thicknesses, the best fit for the PL decay curve was achieved using three exponential components. The “fast” component is characterized by the decay time $\tau_1 \sim 0.5$ –1 ns, the “medium” component decays at the timescale of $\tau_2 \sim 4$ –11 ns, and the “slow” component decays in $\tau_3 \sim 40$ –60 ns. By analyzing the thickness dependence of the relative intensities of these three components and the values of the decay times, we have attributed the “fast” contribution to band-to-band recombination of electrons and holes. The “slow” component is a mixture of an indirect interband transition, when there is a band structure of the “Mexican hat” type, and defect-assisted radiation, whose contribution is significant even in bulk. Consideration of the excitation, relaxation, and recombination of carriers, characteristic of the specific band structure of InSe, based on the group theory allowed us to establish the mechanism for the appearance of a “medium” component in the PL decay. We believe that our results have important implications for the possible fabrication of InSe-based devices.

ACKNOWLEDGMENTS

The work of B.R.B., I.A.E., A.I.G., and M.V.R. was supported by a grant from the Russian Science Foundation (No. 22-22-20049 [59]) and a grant from the St. Petersburg Science Foundation in accordance with Agreement No. 21/2022, dated April 14, 2022.

APPENDIX: METHODS

1. Fabrication of samples

Post-transition-metal chalcogenides can be peeled off by breaking the van der Waals force between adjacent layers. The first example of mechanical exfoliation is a single-layer graphene exfoliated from graphite [2]. For sample preparation, mechanical microcleavage and the so-called adhesive tape method were used. This method consists in sticking the tape on the surface of the material and removing the top layers. Then the tape is folded in half several times. Each time the flakes broke up into thinner parts. Finally, very thin flakes are attached to the PDMS film, which are easily transferred to a

suitable substrate using the HQ graphene 2D crystal transfer system. For simplified transfer, a slight heating of the substrate up to 35 °C is required, which this system easily provides. Flakes consisting of several monolayers were prepared by this technique using bulk β -InSe of good structural quality. Silicon wafers coated with 50-nm-thick gold were used as substrates. In addition, few-layer β -InSe on Si/SiO₂ substrates were studied as reference samples.

2. AFM characterization

The AFM study was carried out on an Ntegra Aura scanning probe microscope (NT-MDT, Russia). To obtain the topography of the samples, high-precision probes HA_NC (NT-MDT, Russia) with a tip curvature radius of less than 10 nm, a resonant frequency of 235 kHz, and a force constant of 12 N/m were used. The surface potential was studied using conductive probes HA_FM/W2C+ (NT-MDT, Russia) with a tip curvature radius of 35 nm, a resonant frequency of 114 kHz, and a force constant of 6 N/m. The surface potential measured in the KPFM method is the difference between the work function of the probe and the sample (i.e., contact potential difference):

$$V_{\text{CPD}}^{\text{Sample}} = (\phi_{\text{Tip}} - \phi_{\text{Sample}})/e.$$

To define the work function of an investigated sample, a reference sample (graphene on SiC [60] or HOPG [61]) with a known work function is used. Thus it is possible to eliminate the volatile work function of the tip and find the work function of the investigated sample using the following equation:

$$\phi_{\text{Sample}} = \phi_{\text{Ref}} + e(V_{\text{CPD}}^{\text{Ref}} - V_{\text{CPD}}^{\text{Sample}}).$$

The approach is detailed in the work of Ref. [62].

3. Raman spectroscopy

For structural characterization of the samples, Raman spectroscopy was used. Micro-Raman measurements were carried out using a Horiba LabRAM HR Evo UV-VIS-NIR-Open spectrometer equipped with a confocal microscope. The measurements were performed at room temperature with continuous-wave (cw) excitation using the 532-nm laser line of a Nd:YAG laser (Laser Quantum Torus). An Olympus MPLN100× objective lens (NA = 0.9) was used for Raman and PL measurements, which allowed us to obtain information from an area with a diameter of ~ 1 μm . To prevent damage to the structures, the incident laser power was limited to 0.4 mW.

4. Micro-photoluminescence spectroscopy

The μ -PL setup was used for optical properties investigation of InSe van der Waals structures. The sample was mounted in a He-flow cryostat ST-500-Attocube with a XYZ piezodriver inside, which allowed us to optimize and precisely maintain the positioning of a chosen place on the sample with respect to a laser spot during a long time period (a few hours). Nonresonant optical excitation of a cw Ti:sapphire laser (710 nm) was used for the μ -PL measurements. Incident radiation was focused in ~ 1 - μm spot on the sample by an

apochromatic objective lens with NA of 0.7. The power density was $\sim 6 \text{ W/cm}^2$. The collected emission was dispersed by a 0.5-m monochromator with a 600/mm grating for the detection of μ -PL spectra at selected wavelengths.

5. Time-resolved photoluminescence spectroscopy

To measure the TRPL spectra, we used a picosecond pulsed semiconductor laser PILAS 405 nm (Advanced Laser

Systems) with repetition frequency of 4 MHz to accurately determine decay times over a large time range. To perform the measurements, we used bandpass filters to completely isolate the PL peak. In all cases, decay curves were measured for the isolated PL peak. A superconducting single-photon detector with a time resolution of about 40 ps and a time-correlated single-photon counting system SPC-130 (Becker Hickl) were chosen for the signal detection.

-
- [1] R. Mas-Balleste, C. Gomez-Navarro, J. Gomez-Herrero, and F. Zamora, 2D materials: To graphene and beyond, *Nanoscale* **3**, 20 (2011).
- [2] A. Geim and I. Grigorieva, Van der Waals heterostructures, *Nature (London)* **499**, 419 (2013).
- [3] A. Chaves, J. G. Azadani, H. Alsalman, D. R. da Costa, R. Frisenda, A. J. Chaves, S. H. Song, Y. D. Kim, D. He, J. Zhou, A. Castellanos-Gomez, F. M. Peeters, Z. Liu, C. L. Hinkle, S.-H. Oh, P. D. Ye, S. J. Koester, Y. H. Lee, P. Avouris, X. Wang *et al.*, Bandgap engineering of two-dimensional semiconductor materials, *npj 2D Mater. Appl.* **4**, 29 (2020).
- [4] Y. Liu, X. Duan, H.-J. Shin, S. Park, Y. Huang, and X. Duan, Promises and prospects of two-dimensional transistors, *Nature (London)* **591**, 43 (2021).
- [5] A. R. P. Montblanch, M. Barbone, I. Aharonovich, M. Atatüre, and A. C. Ferrari, Layered materials as a platform for quantum technologies, *Nat. Nanotechnol.* **18**, 555 (2023).
- [6] P.-H. Ho, Y.-R. Chang, Y.-C. Chu, M.-K. Li, C.-A. Tsai, W.-H. Wang, C.-H. Ho, C.-W. Chen, and P.-W. Chiu, High-mobility InSe transistors: The role of surface oxides, *ACS Nano* **11**, 7362 (2017).
- [7] D. J. Late, B. Liu, J. Luo, A. Yan, H. R. Matte, M. Grayson, C. Rao, and V. P. Dravid, GaS and GaSe ultrathin layer transistors, *Adv. Mater.* **24**, 3549 (2012).
- [8] Y.-Y. Lu, C.-R. Guo, H.-L. Yeh, H.-W. Chen, C.-C. Kuo, J.-H. Hsu, J. Zhou, Y.-T. Huang, S.-H. Hsieh, C.-H. Chen *et al.*, Multilayer GaSe/InSe heterointerface-based devices for charge transport and optoelectronics, *ACS Appl. Nano Mater.* **3**, 11769 (2020).
- [9] J. Chen, S. Cai, R. Xiong, B. Sa, C. Wen, B. Wu, and Z. Sun, High-performance III–VI monolayer transistors for flexible devices, *Phys. Chem. Chem. Phys.* **22**, 7039 (2020).
- [10] K. F. Mak, C. Lee, J. Hone, J. Shan, and T. F. Heinz, Atomically thin MoS_2 : A new direct-gap semiconductor, *Phys. Rev. Lett.* **105**, 136805 (2010).
- [11] G. Wang, A. Chernikov, M. M. Glazov, T. F. Heinz, X. Marie, T. Amand, and B. Urbaszek, Colloquium: Excitons in atomically thin transition metal dichalcogenides, *Rev. Mod. Phys.* **90**, 021001 (2018).
- [12] V. Zólyomi, N. D. Drummond, and V. I. Falko, Band structure and optical transitions in atomic layers of hexagonal gallium chalcogenides, *Phys. Rev. B* **87**, 195403 (2013).
- [13] V. Zólyomi, N. D. Drummond, and V. I. Falko, Electrons and phonons in single layers of hexagonal indium chalcogenides from *ab initio* calculations, *Phys. Rev. B* **89**, 205416 (2014).
- [14] D. V. Rybkovskiy, A. V. Osadchy, and E. D. Obraztsova, Transition from parabolic to ring-shaped valence band maximum in few-layer GaS, GaSe, and InSe, *Phys. Rev. B* **90**, 235302 (2014).
- [15] Y. Guo and J. Robertson, Band structure, band offsets, substitutional doping, and Schottky barriers of bulk and monolayer InSe, *Phys. Rev. Mater.* **1**, 044004 (2017).
- [16] Y. Sun, S. Luo, X.-G. Zhao, K. Biswas, S.-L. Li, and L. Zhang, InSe: A two-dimensional material with strong interlayer coupling, *Nanoscale* **10**, 7991 (2018).
- [17] T. Cao, Z. Li, and S. G. Louie, Tunable magnetism and half-metallicity in hole-doped monolayer GaSe, *Phys. Rev. Lett.* **114**, 236602 (2015).
- [18] A. V. Lugovskoi, M. I. Katsnelson, and A. N. Rudenko, Strong electron-phonon coupling and its influence on the transport and optical properties of hole-doped single-layer InSe, *Phys. Rev. Lett.* **123**, 176401 (2019).
- [19] S. Liu, Y. Yang, F. Yu, X. Wen, Z. Gui, K. Peng, R. Wang, and J. Ying, Pressure-induced superconductivity and nontrivial band topology in compressed γ -InSe, *Phys. Rev. B* **105**, 214506 (2022).
- [20] J. Chen, Phonon-mediated superconductivity in electron-doped monolayer InSe: A first-principles investigation, *J. Phys. Chem. Solids* **125**, 23 (2019).
- [21] J. Chen, X. Wang, and X. Liu, Emergence of superconductivity in an InSe monolayer: Roles of deposited metal and biaxial strain, *J. Phys. Chem. Solids* **168**, 110823 (2022).
- [22] K. Iordanidou, M. Houssa, J. Kioseoglou, V. Afanas'ev, A. Stesmans, and C. Persson, Hole-doped 2D InSe for spintronic applications, *ACS Appl. Nano Mater.* **1**, 6656 (2018).
- [23] H. Arora and A. Erbe, Recent progress in contact, mobility, and encapsulation engineering of InSe and GaSe, *InfoMat* **3**, 662 (2021).
- [24] T.-H. Tsai, F.-S. Yang, P.-H. Ho, Z.-Y. Liang, C.-H. Lien, C.-H. Ho, Y.-F. Lin, and P.-W. Chiu, High-mobility InSe transistors: The nature of charge transport, *ACS Appl. Mater. Interfaces* **11**, 35969 (2019).
- [25] K. Premasiri, S. K. Radha, S. Sucharitakul, U. R. Kumar, R. Sankar, F.-C. Chou, Y.-T. Chen, and X. P. Gao, Tuning Rashba spin-orbit coupling in gated multilayer InSe, *Nano Lett.* **18**, 4403 (2018).
- [26] J. Liu, W. Kang, T.-Y. Zhou, and C.-G. Ma, Graphene-like monolayer InSe–X: Several promising half-metallic nanosheets in spintronics, *J. Phys.: Condens. Matter* **30**, 155306 (2018).
- [27] Y. Wang, J. Gao, B. Wei, Y. Han, C. Wang, Y. Gao, H. Liu, L. Han, and Y. Zhang, Reduction of the ambient effect in

- multilayer InSe transistors and a strategy toward stable 2D-based optoelectronic applications, *Nanoscale* **12**, 18356 (2020).
- [28] Z. Chen, C. Giorgetti, J. Sjakste, R. Cabouat, V. Véniard, Z. Zhang, A. Taleb-Ibrahimi, E. Papalazarou, M. Marsi, A. Shukla, J. Peretti, L. Perfetti *et al.*, Ultrafast electron dynamics reveal the high potential of InSe for hot-carrier optoelectronics, *Phys. Rev. B* **97**, 241201(R) (2018).
- [29] L. Zhang, Z. Li, J. Yang, J. Zhou, Y. Zhang, H. Zhang, and Y. Li, A fully integrated flexible tunable chemical sensor based on gold-modified indium selenide nanosheets, *ACS Sens.* **7**, 1183 (2022).
- [30] L. Wu, J. Shi, Z. Zhou, J. Yan, A. Wang, C. Bian, J. Ma, R. Ma, H. Liu, J. Chen *et al.*, InSe/hBN/graphite heterostructure for high-performance 2D electronics and flexible electronics, *Nano Res.* **13**, 1127 (2020).
- [31] W. Ibarra-Hernández, A. C. Garcia-Castro, A. Bautista-Hernández, M. Salazar-Villanueva, A. Cantarero, and A. H. Romero, Modification of electronic and thermoelectric properties of InSe/GaSe superlattices by strain engineering, *Phys. Rev. Mater.* **6**, 025403 (2022).
- [32] D. Maeso, S. Pakdel, H. Santos, N. Agraït, J. J. Palacios, E. Prada, and G. Rubio-Bollinger, Strong modulation of optical properties in rippled 2D GaSe via strain engineering, *Nanotechnology* **30**, 24LT01 (2019).
- [33] Y. Li, T. Wang, M. Wu, T. Cao, Y. Chen, R. Sankar, R. K. Ulaganathan, F. Chou, C. Wetzel, C.-Y. Xu *et al.*, Ultrasensitive tunability of the direct bandgap of 2D InSe flakes via strain engineering, *2D Mater.* **5**, 021002 (2018).
- [34] C. Wang, Y. Liu, J. Yuan, P. Wu, and W. Zhou, Scaling law of hydrogen evolution reaction for InSe monolayer with 3D transition metal doping and strain engineering, *J. Energy Chem.* **41**, 107 (2020).
- [35] D. K. Sang, H. Wang, M. Qiu, R. Cao, Z. Guo, J. Zhao, Y. Li, Q. Xiao, D. Fan, and H. Zhang, Two dimensional β -InSe with layer-dependent properties: Band alignment, work function and optical properties, *Nanomaterials* **9**, 82 (2019).
- [36] C. Song, S. Huang, C. Wang, J. Luo, and H. Yan, The optical properties of few-layer InSe, *J. Appl. Phys.* **128**, 060901 (2020).
- [37] G. W. Mudd, M. R. Molas, X. Chen, V. Zólyomi, K. Nogajewski, Z. R. Kudrynskiy, Z. D. Kovalyuk, G. Yusa, O. Makarovskiy, L. Eaves, M. Potemski, V. I. Fal'ko, and A. Patané, The direct-to-indirect band gap crossover in two-dimensional van der Waals indium selenide crystals, *Sci. Rep.* **6**, 39619 (2016).
- [38] D. A. Bandurina, A. V. Tyurnina, G. L. Yu, A. Mishchenko, V. Zólyomi, S. V. Morozov, R. K. Kumar, R. V. Gorbachev, Z. R. Kudrynskiy, S. Pezzini, Z. D. Kovalyuk, U. Zeitler, K. S. Novoselov, A. Patané, L. Eaves, I. V. Grigorieva, V. I. Fal'ko, A. K. Geim, and Y. Cao, High electron mobility, quantum Hall effect and anomalous optical response in atomically thin InSe, *Nat. Nanotechnol.* **12**, 223 (2017).
- [39] G. W. Mudd, S. A. Svatek, T. Ren, A. Patané, O. Makarovskiy, L. Eaves, P. H. Beton, Z. D. Kovalyuk, G. V. Lashkarev, Z. R. Kudrynskiy, and A. I. Dmitriev, Tuning the bandgap of exfoliated InSe nanosheets by quantum confinement, *Adv. Mater.* **25**, 5714 (2013).
- [40] T. Zheng, Z. T. Wu, H. Y. Nan, Y. F. Yu, A. Zafar, Z. Z. Yan, J. P. Lu, and Z. H. Ni, Layer-number dependent and structural defect related optical properties of InSe, *RSC Adv.* **7**, 54964 (2017).
- [41] T. Venanzi, H. Arora, S. Winnerl, A. Pashkin, P. Chava, A. Patane, Z. D. Kovalyuk, Z. R. Kudrynskiy, K. Watanabe, T. Taniguchi, A. Erbe, M. Helm, and H. Schneider, Photoluminescence dynamics in few-layer InSe, *Phys. Rev. Mater.* **4**, 044001 (2020).
- [42] M. J. Hamer, J. Zultak, A. V. Tyurnina, V. Zólyomi, D. Terry, A. Barinov, A. Garner, J. Donoghue, A. P. Rooney, V. Kandyba *et al.*, Indirect to direct gap crossover in two-dimensional InSe revealed by angle-resolved photoemission spectroscopy, *ACS Nano* **13**, 2136 (2019).
- [43] T. V. Shubina, W. Desrat, M. Moret, A. Tiberj, O. Briot, V. Y. Davydov, A. V. Platonov, M. A. Semina, and B. Gil, InSe as a case between 3D and 2D layered crystals for excitons, *Nat. Commun.* **10**, 3479 (2019).
- [44] C. Zhao, W. Yan, S. Han, W. Zhang, M. Jin, and D. Liu, Mechanically accessible band engineering via indentation-induced phase transition on two-dimensional layered β -InSe, *Appl. Surf. Sci.* **604**, 154573 (2022).
- [45] S. J. Magorrian, V. Zólyomi, and V. I. Fal'ko, Electronic and optical properties of two-dimensional InSe from a DFT-parametrized tight-binding model, *Phys. Rev. B* **94**, 245431 (2016).
- [46] K. J. Xiao, A. Carvalho, and A. H. Castro Neto, Defects and oxidation resilience in InSe, *Phys. Rev. B* **96**, 054112 (2017).
- [47] F.-S. Yang, M. Li, M.-P. Lee, I.-Y. Ho, J.-Y. Chen, H. Ling, Y. Li, J.-K. Chang, S.-H. Yang, Y.-M. Chang *et al.*, Oxidation-boosted charge trapping in ultra-sensitive van der Waals materials for artificial synaptic features, *Nat. Commun.* **11**, 2972 (2020).
- [48] Y. Zhang, X. Sun, K. Jia, H. Yin, K. Luo, J. Yu, and Z. Wu, Enhancement of InSe field-effect-transistor performance against degradation of InSe film in air environment, *Nanomaterials* **11**, 3311 (2021).
- [49] I. Grimaldi, T. Gerace, M. Pipita, I. Perrotta, F. Ciuchi, H. Berger, M. Papagno, M. Castriota, and D. Pacilé, Structural investigation of InSe layered semiconductors, *Solid State Commun.* **311**, 113855 (2020).
- [50] R. Boyd, *Nonlinear Optics* (Academic Press, New York, 2020).
- [51] C. Carlone, S. Jandl, and H. Shanks, Optical phonons and crystalline symmetry of InSe, *Phys. Status Solidi B* **103**, 123 (1981).
- [52] M. R. Molas, A. V. Tyurnina, V. Zólyomi, A. K. Ott, D. J. Terry, M. J. Hamer, C. Yelgel, A. Babiński, A. G. Nasibulin, A. C. Ferrari *et al.*, Raman spectroscopy of GaSe and InSe post-transition metal chalcogenides layers, *Faraday Discuss.* **227**, 163 (2021).
- [53] S. Lei, L. Ge, S. Najmaei, A. George, R. Kappera, J. Lou, M. Chhowalla, H. Yamaguchi, G. Gupta, R. Vajtai *et al.*, Evolution of the electronic band structure and efficient photo-detection in atomic layers of InSe, *ACS Nano* **8**, 1263 (2014).
- [54] D. G. Hopkinson, V. Zólyomi, A. P. Rooney, N. Clark, D. J. Terry, M. Hamer, D. J. Lewis, C. S. Allen, A. I. Kirkland, Y. Andreev *et al.*, Formation and healing of defects in atomically thin GaSe and InSe, *ACS Nano* **13**, 5112 (2019).
- [55] I. A. Elisayev, A. I. Galimov, M. V. Rakhlin, E. Evropeitsev, A. Toropov, V. Y. Davydov, S. Thiele, J. Pezoldt, and T. Shubina, Photoluminescence kinetics of dark and bright excitons in atomically thin MoS₂, *Phys. Status Solidi RRL* **15**, 2100263 (2021).

- [56] Y. Li, Y. Rao, K. F. Mak, Y. You, S. Wang, C. R. Dean, and T. F. Heinz, Probing symmetry properties of few-layer MoS₂ and h-BN by optical second-harmonic generation, *Nano Lett.* **13**, 3329 (2013).
- [57] Z. Sun, Y. Zhang, J. Qian, R. Qiao, X. Li, Z. Wang, C. Zheng, K. Liu, T. Cao, W.-T. Liu, and S. Wu, Compelling evidence for the ϵ -phase InSe crystal by oblique incident second harmonic generation, *Adv. Opt. Mater.* **10**, 2201183 (2022).
- [58] N. Kuroda, I. Munakata, and Y. Nishina, Exciton transitions from spin-orbit split off valence bands in layer compound InSe, *Solid State Commun.* **33**, 687 (1980).
- [59] <https://rscf.ru/project/22-22-20049/>.
- [60] V. Panchal, R. Pearce, R. Yakimova, A. Tzalenchuk, and O. Kazakova, Standardization of surface potential measurements of graphene domains, *Sci. Rep.* **3**, 2597 (2013).
- [61] W. N. Hansen and G. J. Hansen, Standard reference surfaces for work function measurements in air, *Surf. Sci.* **481**, 172 (2001).
- [62] B. Borodin, F. Benimetskiy, I. Nyapshaev, and P. Alekseev, Kelvin probe force gradient microscopy of WSe₂ monolayers on Ni, *J. Phys.: Conf. Ser.* **1400**, 055012 (2019).